Instrument Science Report WFC3 2015-14

WFC3 IR Gain from 2010 to 2015

C. M. Gosmeyer & S. Baggett
September 09, 2015

ABSTRACT

The conversion from electronic analog data units (ADUs) to electrons is one of the fundamental parameters needed to characterize the IR channel of WFC3. The IR detector on WFC3 has four quadrants, each with a separate amplifier chain. Here we report measurements of the gain of each of the amplifiers using a set of internal flat fields (F126N, SPARS50, 13 reads, ~600 sec). We find the gain values to be 2.27, 2.21, 2.20, 2.28 ± 0.02 e-/ADU for quadrants 1, 2, 3, 4, respectively. The flat field observations were taken from Oct. 2010 to June 2015 at a nominal gain setting of 2.5 e-/ADU. Persistence seems to have had little effect on our gain measurement, although it emerged unexpectedly at just half full-well in some of our flat fields (~14,000 DN/pix). Finally we compare the gain values computed from data calibrated with the current pipeline (2008) non-linearity correction to those computed from data calibrated with the new 2014 correction and find the difference, <1%, is negligible.

1.0 Introduction

The WFC3/IR channel consists of a low-noise, high-QE, 1024x1024 pixel HgCdTe array, divided into four 512x512 quadrants, each with its own readout amplifier. It has a nominal gain setting of 2.5 e-/ADU. However, the actual gain values for the detector's quadrants are different due to slight differences in the electronics hardware. A key characteristic of the detector, the gain is propagated into WFC3/IR's data reduction pipeline, providing the factor for converting science data into units of electrons. The gain, routinely monitored on-orbit, can also provide insight into the health and stability of the detector.

In this report we describe the results of the calibration program to measure the gain in each of the detector's quadrants and the various tests we performed to check our data for persistence and unintentional biases from our analysis methods. The final gain values are tabulated in

Section 3.5 both for data with the current (2008) and the 2014 non-linearity corrections. We also list the gain values obtained without the inter-pixel capacitance (IPC) correction applied.

2.0 Data

A calibration program to routinely measure the IR gain has been in place since launch. Starting in Cycle 18, this yearly program consists of 16 identical one-orbit visits, each containing a dark current observation, a short warm-up flat, and a long flat. Each cycle is scheduled so that half (eight visits) are observed in a space of a few days every six months. The visits are never taken back-to-back in order to avoid self-induced persistence. The observing strategy in the first year of WFC3 on-orbit operations (Cycle 17) was different, consisting of different iterations of RAPID, SPARS25, and SPARS10 sample sequences of the Tungsten lamp, taken in filters F140W, F139M, and F153M, respectively. No preceding darks were taken each visit. We do obtain gain values from them, but keeping in mind that they cannot be directly compared to values obtained from the subsequent cycles' data.

A visit starts with a short dark current observation, which serves as a check on any persistence present on the detector from previous observations. Next the Tungsten lamp is turned on and a short flat field is observed to give the lamp time to reach a stable flux output. A narrowband filter (F126N), which collects ~1200 DN/pix, is set here to reduce the chance of persistence in the next ramp. Finally the longer flat field ramp is observed. This is the observation we use in the gain measurement. The flat is designed to collect ~14,000 DN/pix, about half of full-well, with the purpose to minimize the non-linearity correction needed later in the analysis. Furthermore, keeping our exposure levels at half full-well should minimize any adverse effects due to persistence, or afterglows, which arise when flux levels approach saturation (Long et al. 2010). However, as we discuss in Section 3.3, we have in the course of preparing this report learned that half full-well may still be too high to mitigate afterglows. Table 1 summarizes the properties of a nominal visit. Table 2 lists all the gain monitor programs up to 2015 and their dates of observation.

Table 1. A nominal visit of the IR gain monitor. Sixteen identical visits are observed each year.

Label	Target	Filter	SAMP-SEQ	NSAMP (# reads)	Exp. Time (s)
Dark	DARK-NM[1]	BLANK	SPARS10	9	82.94
Warm-up (short) Flat	TUNGSTEN	F126N	SPARS10	6	52.937
Gain (long) Flat	TUNGSTEN	F126N	SPARS50	13	602.938

[1]"DARK-NM" is a dark with the blank in place, but to minimize channel select mechanism (CSM) use the CSM is not moved (NM) between the previous exposure and the dark.

Table 2. CAL Programs for the IR gain monitor.

Cycle	Program	Visits 1-8	Visits 9-16
17[1]	11930	-	-
18	12350	30,31 Oct. 2010	30 Nov. 2010
19	12697	17,18,19 Oct. 2011	26,28 Feb. & 1,2,3 Mar. 2012
20	13080	18,19,20 Oct. 2012	4,5,6,7 July 2013
21	13564	4,6,8 Nov. 2013	2,3,4 June 2014
22[2]	14010	11,12,13,14 Nov. 2014	1,2, 29 June 2015

[1]As described in the text, the Cycle 17 data were taken at a different cadence. [2]In Cycle 22, only four of the eight visits scheduled for early June 2015 were observed due to an anomalous (safing) event. The remaining four visits were rescheduled and taken later in the month. They are actually archived as Visits 17-20.

3.0 Analysis

For the analysis, we use IMA FITS files, which are intermediate ramps generated by CALWF3 that contain the full stack of calibrated reads with the zeroth read subtracted. Calibrations include subtracting dark current, identifying cosmic rays, correcting for non-linearity, and so on. All pre-June 2015 files were retrieved from MAST in March 2015 and processed with CALWF3 Version 3.1.6 with UNITCORR set to 'omit'. Omitting UNITCORR ensures that units remain in counts, not countrates. See the WFC3 Data Handbook, Section 3.4, for additional information on the calibration steps (Rajan et al. 2010).

3.1 Theory

To calculate the gain with our flat fields we implement the mean-variance method, which is commonly used for CCDs and other devices, and whose description we reproduce here from Baggett (2005) and Hilbert (2005). Because we must sift out sources of noise to identify the gain, we must in practice use differenced ramps instead of the flat fields themselves. It is desirable, then, that the two ramps in the differenced ramp be as similar as possible – we go into further detail in the next section. In the mean-variance method we assume that in the differenced ramp there are only two sources of noise: read noise (RN) and photon noise (P). Then the total noise (N) is found by

$$(N/g)^2 = (P/g)^2 + (RN/g)^2 ,$$

where g is the gain in units of e-/ADU. Noise is in units of e-.

Photon noise is the square root of the product of the mean signal (μ) and the gain. The total noise is the image's observed variance (σ^2). The mean is in units of ADU and the variance is in units of ADU^2. Then observed variance can be written as

$$\sigma^2 = (1/g)* \mu + (R/g)^2 .$$

The gain is the inverse slope of the linear least squares fit to the plot of variances versus means.

3.2 Implementation

We use IDL scripts, based on scripts written by B. Hilbert and still reliant on procedures from his personal library, to apply the mean-variance method to pairs of ramps. The primary idea is to sum and difference pairs of ramps, read-by-read, and from these summed and differenced ramps calculate the mean and variance for each read. Each ramp is paired to a ramp that was taken within 24 hours. If no match is found the ramp is tossed out. See Tables A1 and A2 in the Appendix for the list of pairs. Note that although the strict 24-hour matching was not the procedure used in previous analyses, we find that this restriction gives us the most stable results because the ramps are more similar. In calibration proposals going forward, we will request the pairs always be taken within a day of each other, although they cannot be taken back-to-back because of the possibility of self-persistence.

As a pair goes through the software, it is first corrected for the effect of inter-pixel capacitance (IPC). This effect is seen in IR detectors as a "smoothing" of a single pixel's charge across several pixels and has been known to artificially increase the actual gain measurements (Hilbert & McCullough 2011, Hilbert 2008). To correct for IPC, we use a deconvolution script written by P. McCullough and described in his 2008 ISR. The IPC kernel is a 3x3 matrix, where about 6% of the flux from a pixel is distributed into the surrounding pixels, the majority going into the pixels directly above, below, left, and right.

Next we mask (set to NaN) the following:

- The image border (a five-pixel rind).
- The glow in the upper edge of quadrant 1.
- The "Death Star" and the anomalous area to its right in quadrant 2.
- The "Wagon Wheel" in quadrant 3.
- Marked bad pixels.

Note that the quadrants are numbered 1 to 4, counterclockwise from the upper left. See the WFC3 Instrument Handbook (Dressel 2015), Section 5.7, for more details on the IR detector's cosmetics.

With the IPC correction and masking complete, the script sums and differences the ramp pair pixel-by-pixel, read-by-read. They are 3-sigma clipped to remove outliers. Using these summed and differenced ramps, the mean and variance for each quadrant of each read is calculated. Each quadrant is, in turn, divided into a 25x25 grid; this significantly speeds up the code and allows bad areas of the detectors to be thrown out via another 3-sigma clipping on the grid's squares. For each square of each ramp the mean is plotted against the variance. Finally, the slope is taken; the inverse of this slope is the gain. See Figure 1 for an example mean-variance plot.

The slope varies slightly from pair to pair, yielding gain values that differ at most by 3% within a quadrant. On average, the values match within 1-2%. There seem to be similarities between values quadrant-to-quadrant. Gains from quadrants 1 and 4 match each other well (within 1%). Similarly, quadrants 2 and 3 show a good match, also within 1%. The quadrants' symmetry is an

interesting coincidence; at present we do not have a physical reason for why this might be, since it is quadrants 1 & 2 and 3 & 4 that are electronically connected. In Section 3.5 we report how we define "final" gains for each quadrant from all the ramp pairs.

Uncertainties (listed in Tables A1 and A2) in each pair's gain are found using the estimated standard deviations of the coefficients output by an IDL line-fitting routine ROBUST_LINEFIT. The calculation is sketched below.

First the differenced pair's gain is found from the mean-variance slope's reciprocal.

gain = 1 / slope

Then the upper and lower gain offsets are found.

upper_offset = 1 / (slope + estimated_standard_dev)

lower_offset = 1 / (slope - estimated_standard_dev)

Finally the gain uncertainty is calculated from the max of the absolute values of the upper and lower offsets subtracted from the gain.

gain_uncertainty = max[abs(gain - upper_offset), abs(gain - lower_offset)]

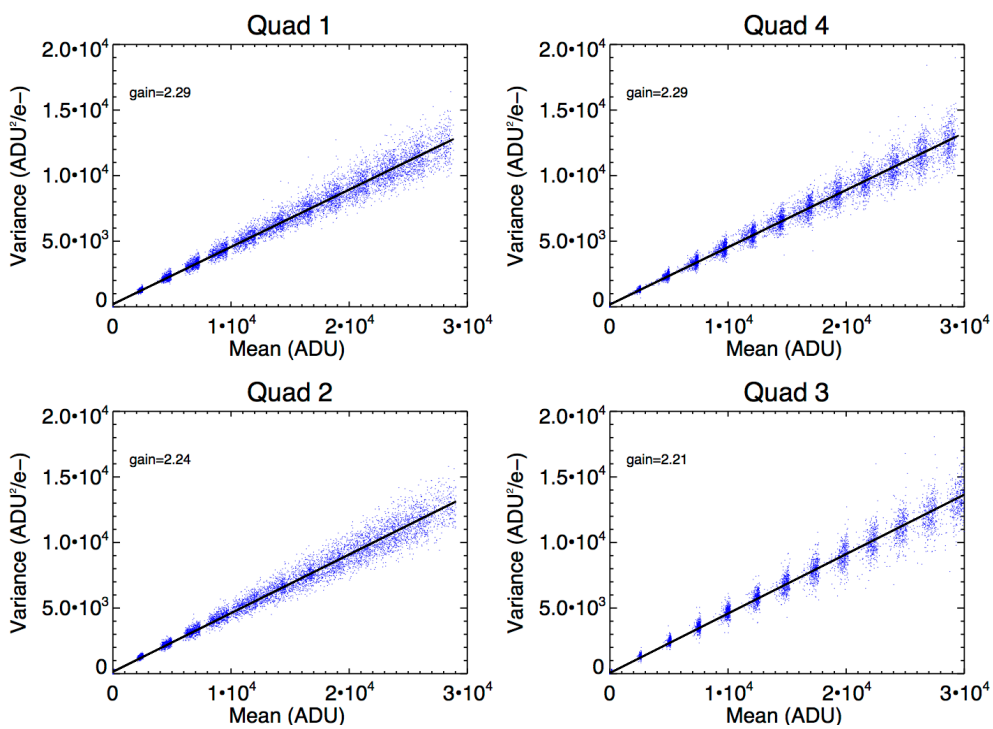

Figure 1. Example of a mean-variance plot for a single ramp pair taken with 13 reads and the SPARS50 sample sequence. This pair displayed here is *ibve03lnq_ima.fits* and *ibve04mpq_ima.fits*.

3.3 Tests

We performed various tests to sanity-check our values and method, which was adapted with modification from B. Hilbert.

Relaxing the Definition of a "Ramp Pair"

We looked into calculating the gain where we allowed ramps to be paired if they were taken within 48 hours of each other. This relaxation increased our selection; however, it also appeared to increase the uncertainty. The gain values from these more liberally defined pairs are 1-2% less than the pairs that matched within 24 hours. Therefore we decided to stay within a 24-hour selection. Note that visits are never taken back-to-back in order to avoid self-persistence.

Changing Grid Size

As described in Section 3.2, we chop each quadrant of the summed and differenced ramps into a 25x25 grid. In each square the mean and variance are calculated. If the square happens to consist predominantly of masked pixels, the gain calculation could have a larger uncertainty, and so, the software is built to throw out bad squares via a 3-sigma clipping. But as a sanity-check – in case too many squares were being tossed away – we ran the scripts with increased box sizes, yielding a 5x5 grid.

Figure 2 illustrates the results with linear fits to mean-variance plots of a ramp pair sliced with the two grid sizes. It is apparent increasing the grid size has little effect (other than increasing the CPU time) – gain values are higher by less than 0.5% in quadrants 1, 2, and 4. Quadrant 3, containing the large anomalous area known as the "Wagon Wheel", shows an increase of ~1.5%. Therefore we conclude anomalous portions of the detector are not badly skewing our results, but we should allow for more uncertainty in the gain values we acquire for quadrant 3.

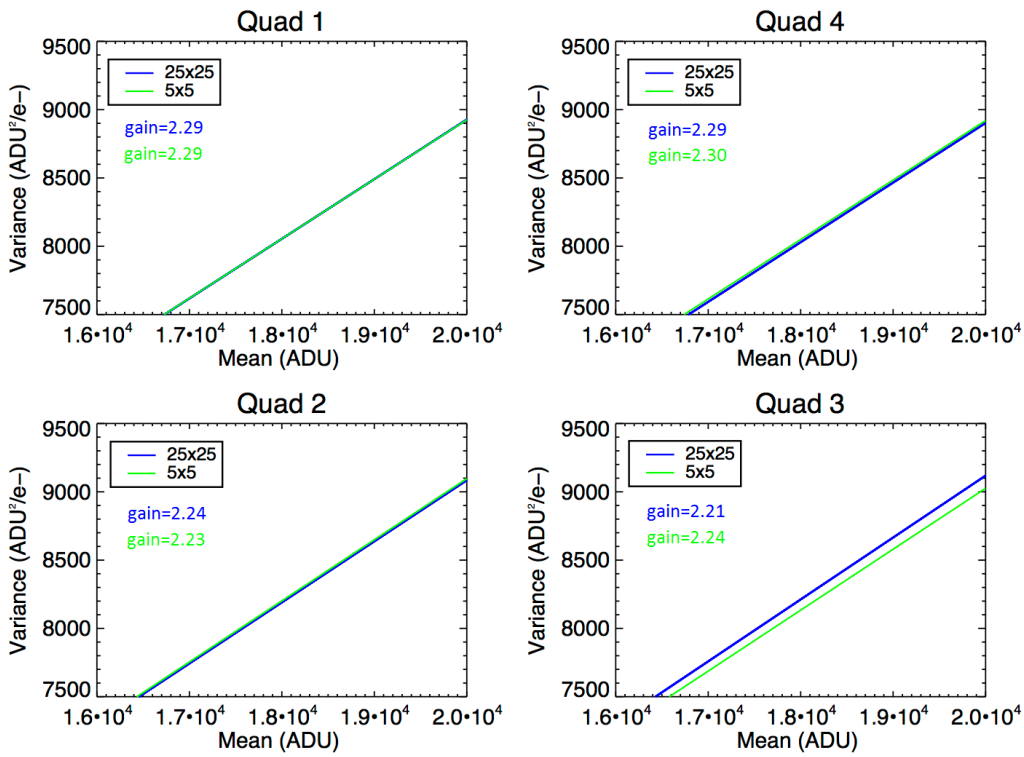

Figure 2. A close-up view of the least-squares linear fits to the mean-variance plots of the ramp pair *ibve03lnq_ima.fits* and *ibve04mpq_ima.fits*, in which the quadrants are divided into a 25x25 grid (as show in Figure 1) and a 5x5 grid. The difference is miniscule and really only apparent in quadrant 3, which contains heavy masking due to the "Wagon Wheel."

Persistence Checks: Short Flat Ratios

We were suspicious that our results could be skewed if persistence, an additive effect, were present. To check for persistence, we examined the short flats first by eye, and then by ratio-ing them, read-by-read, to a common early flat from our dataset (*ibm802h9q_ima.fits* from Cycle 18, CAL Program 12350). By eye we did not see obvious persistence. And this was confirmed by the median ratios shown in Figure 3: there is a gentle slope downward, but no extreme outliers. We repeated the ratios using different Cycle 18 flats and obtained corroborating results. In fact, the plots' steady decrease is consistent with Ryan & Baggett (2015), which reports finding a ~0.3% per year decrease in the IR internal flat lamp output. Similarly, in the UVIS "bowtie" monitor (the UVIS and IR lamps are from the same manufacturing batch and hence we expect similar behaviors), the lamp's output is found to have decreased by ~1% over WFC3's lifetime (Bourque & Baggett 2013).

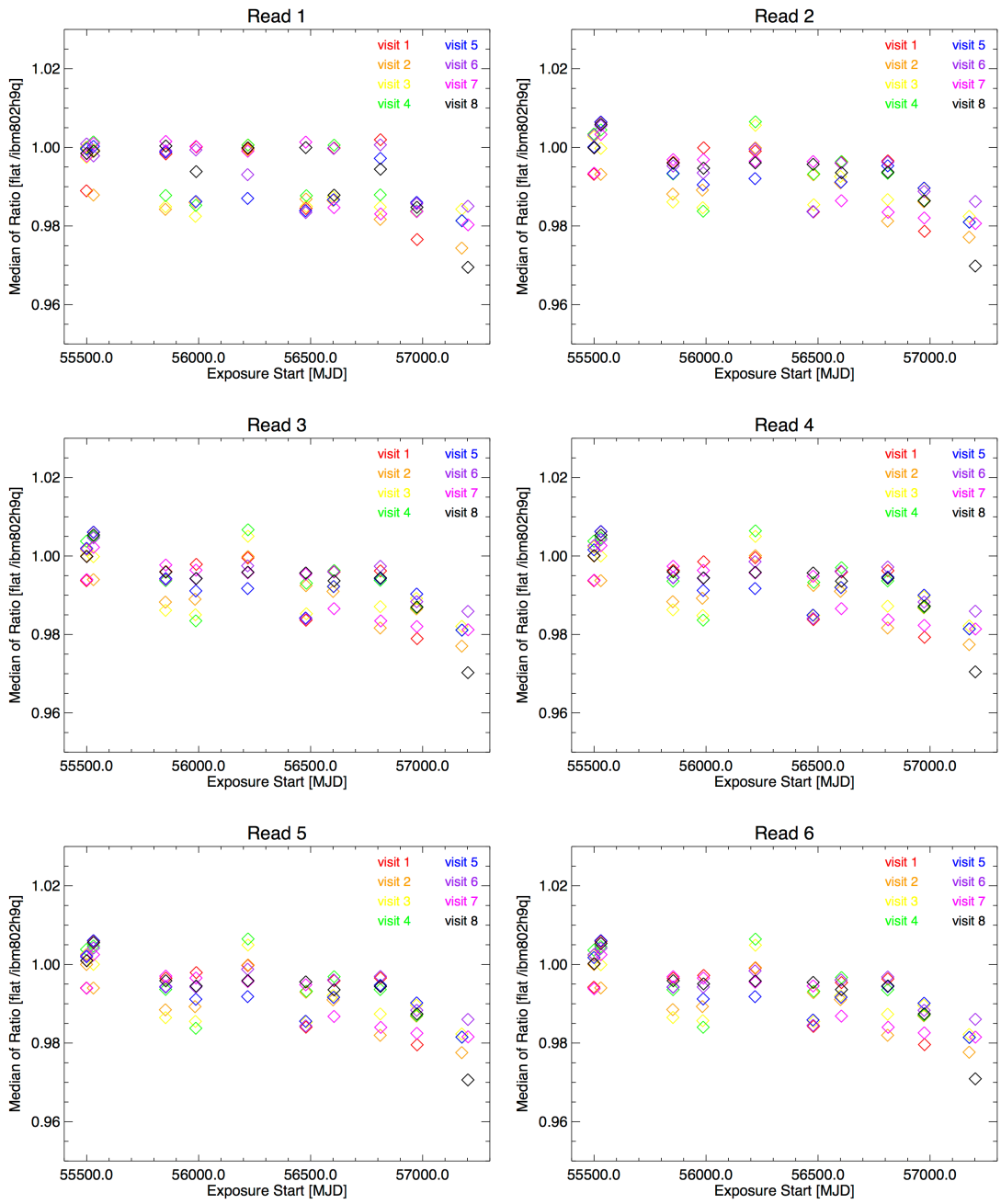

Figure 3. Medians of the short (6-read) flats' ratio to the Cycle 18, Program 12350 flat *ibm802h9q_ima.fits*. Each panel shows a different read, and each color shows a different visit in the eight-visit per six-month observation cadence. If a large amount of persistence were present, we would expect outliers. Because all points remain within 1% of their eight-visit cluster, we believe persistence is not a concern in this dataset.

Persistence Checks: Long Flats Ratios

However, when we did the same ratio-ing tests with the long flats (using *ibm802haq_ima.fits* from Cycle 18, CAL Program 12350), we found signs of persistence on about 30% of the flats. This was unexpected. We had assumed our leading darks and short flats would pick up any persistence, and if they were clean, so would be the long flats. Moreover, the long flats reached only half-full-well at the last reads, ~14,000 DN/pix, which we had expected to be low enough to avoid persistence (Long et al. 2010). This phenomenon of afterglow appearing after multiple persistence-free images has occasionally been seen on-orbit and been dubbed "burping". In those anecdotal accounts, the "burping" seemed to follow significantly-exposed flat fields; in the case of the IR gain data, the flat field levels are only ~1/2 full-well. An analysis of the internal flat field monitoring data, where exposure levels are much closer to full-well, showed long-term persistence, or "burping," effects in nearly 2/3 of the images (Ryan & Baggett 2015). This detector behavior will be worth further investigation. For the present, we needed to evaluate what effect the persistence was having on our gain measurements, and whether we needed to toss out contaminated pairs from the dataset.

To that end, we looked through each of the long flat ratios and flagged each quadrant of each image in which we found a persisting object, using the flagging scheme defined below. Figure 5 shows examples, and Table 6 in the Appendix lists the flags for each file in our dataset.

0 — Clean. No persistence apparent.
1 — Minimal persistence, small area affected, offset in gain measurement not expected. (Up to five streaks from grisms, a persisted star or two, etc.)
2 — Larger areas affected, might be skeptical of gain measurement. (All these were determined to be light scattering, not actually persistence.)
3 — Bad, widespread persistence. Image probably should be thrown out.

We plot the gain values from Table A2 against image index (Figure 6) and then against time (Figure 7), coding each of the flags by color and marker type. We do not see a trend in gain with persistence, except in the one extreme outlier at ~1.9 e-/DN. A look at the ratio image of one of the ramps (*ibve16o1q_ima.fits*) in the pair used in the outlier's gain calculation reveals a star field persisting across the entire frame of the detector. This is the worst case of persistence we have seen in the dataset; none other comes near to being so prevalent. Based on the somewhat random distribution of persistence flags among the clean data, we conclude persistence is not, except in the one extreme case, causing our gain measurements to be offset. See Figure 12 in the Appendix for median ratio plots, similar to Figure 3, for each ramp of the long flats.

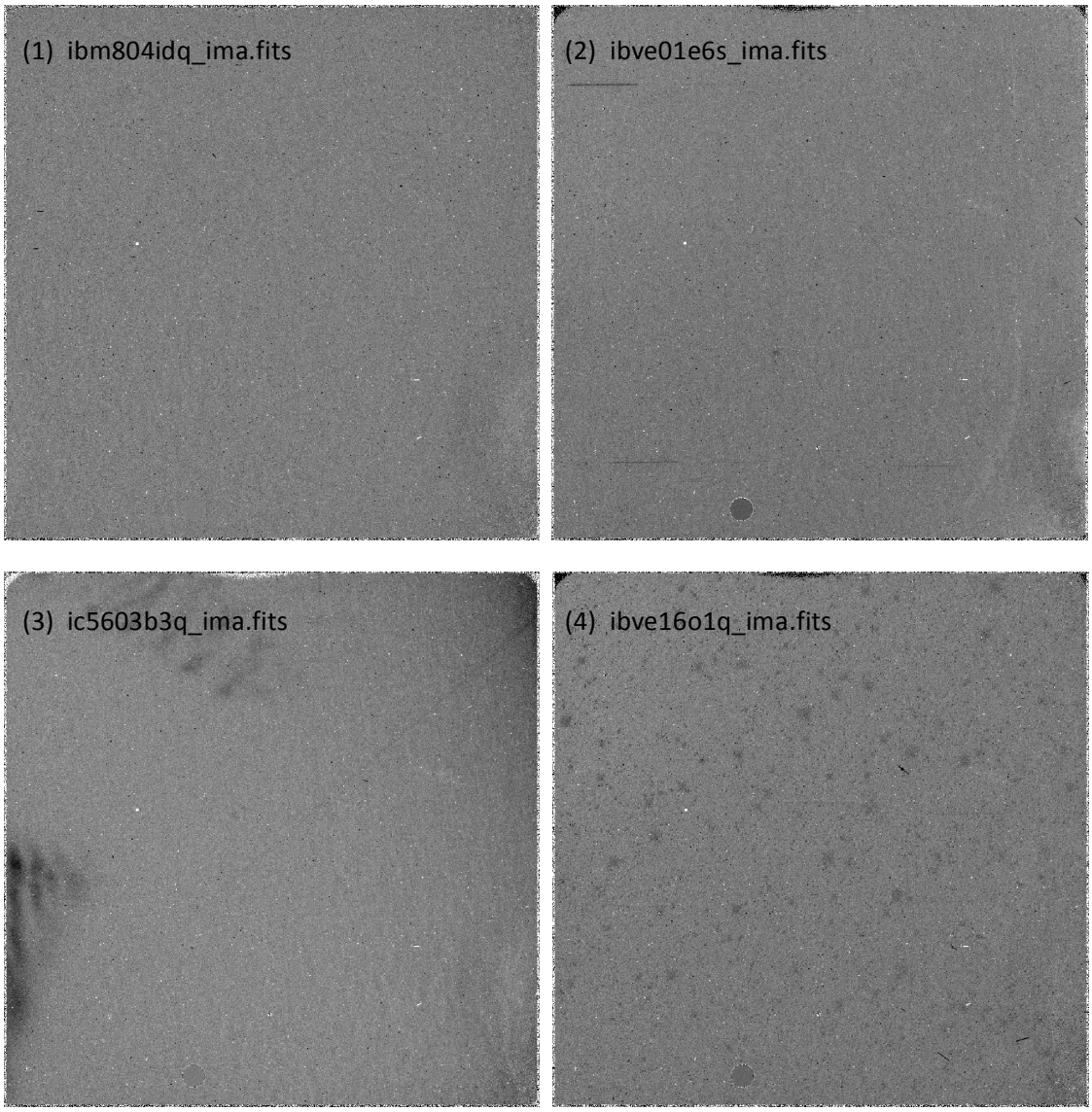

Figure 5. The four panels, showing ratios of the labeled images, give examples of the four persistence "flags" we applied to sort our long flats. Panel (1) shows a clean ratio without persistence (our "flag=0"). Panel (2) shows a ratio with at least three persisting grism trails, "flag=1". Panel (3), an example of "flag=2" is, in fact, not persistence, but rather a light scattering effect in the internal flat fields known as "glinting" (Baggett 2009). Our plots in Figures 6 and 7 show that glinting does not appear to have impacted our gain measurements. Finally panel (4) shows our worst case of persistence, discussed in the text, in which the entire frame is sprayed with a star field. Each contaminated pixel has anywhere from a few to a few hundred more DN than nearby non-contaminated pixels. Visible in panels (2), (3), and (4) are flat field features such as the "Death Star" and "Wagon Wheel", as well as the vertical line feature in the upper right of (2).

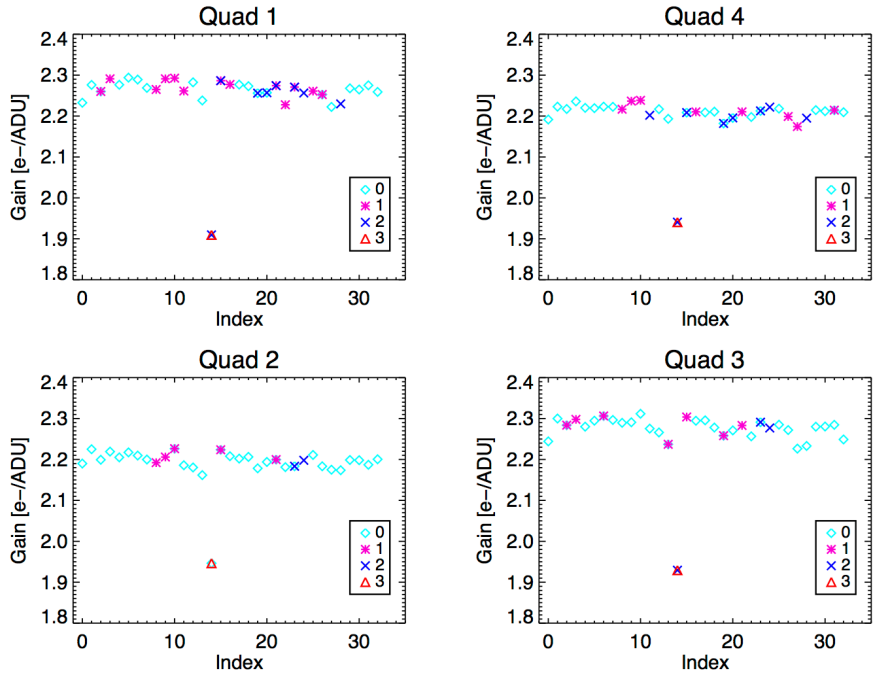

Figure 6. Gain plotted against index, with persistence flags coded in color and marker shape. The standard deviation for each quadrant's gain (discarding the outlier) is about 0.02. Note that each ramp within a pair is plotted and overlaps, since indexing is done by ramp pair, not by individual ramps. Because the flagged points are scattered both high and low among the unflagged points, there does not seem to be a trend with gain. See the text for discussion on the "flag 3" outlier.

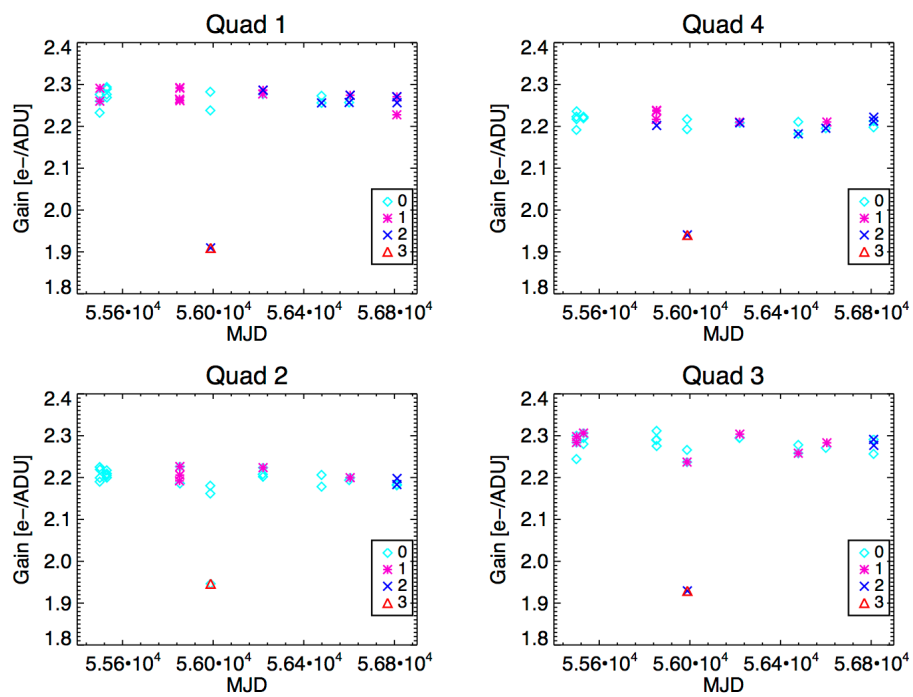

Figure 7. Similar to Figure 6, but with gain plotted against time, allowing a view of the trend with visit. See Figure 6 for a less impeded view of the points. Again, because the flagged points distribute randomly among the clean points, there does not seem to be a trend with gain.

Short vs. Long Flats

Out of our concern over persistence, we ran the gain scripts over both the short flats (6 reads) and the long flats (13 reads). The results do vary, where the gain values are smaller for the 6-read ramps. (See Tables 4 and 5 in the Appendix for gain values for each ramp pair.) We initially attributed this divergence to persistence; however, exposure levels well below saturation should not cause persistence significant enough to offset the values so severely (Long et al. 2010), and, indeed, our checks described in the previous section ruled out such persistence. We then suspected that the gain might be changing based on where along the mean-variance plot the measurement is taken. This is described next.

Decreasing the Number of Reads

Taking the RAW FITS of each of our 13-read ramps, we chopped off a read and calibrated the new, shorter 12-read ramp with CALWF3 to obtain a 12-read IMA and ran it as usual through the gain script. This chopping and recalibrating was repeated with 11 reads, then with 10 reads, and so on, until the number of reads reached two. We had in the end 11 different values of the gain for each number of the reads. As Figure 8 shows, decreasing the number of reads in our 13-read flats pushes the average gain values closer and closer to that from the six-read flats. From this we conclude that persistence is not responsible for the difference in the gain values in the short and long flats. The cause, instead, may be that a different height of the mean-variance line is being sampled. Given that there is no obvious sweet-spot for the gain value, we choose to measure it using the 13-read SPARS50 internal flats.

The initial purpose of Figure 8 was to show that as the recalibrated SPARS50 reads decrease, the mean gain approaches that for the 6-read SPARS10 data. However, the plot has raised further questions and initiated additional testing. For instance, it is curious that after the first six reads of the blue markers (any before six can be disregarded because the signal is so low) there is still a steady rise in the gain measurement with number of reads used. We believe this is a consequence of the gain measurement itself. From plots such as the examples shown in Figures A2 and A3, we find that the variance/exposure time changes by as much as 90% from pairs calculated from two-read flats to 13-read flats. The mean/exposure time remains steady, however, from two-read to 13-reads, save for a 0.5% decline with increasing number of reads, which we attribute to the imperfection of the non-linearity correction. The variance's behavior with number of reads will require further investigation; for the gain calculation it does not matter as long as we are consistent in our choice of sample sequence and total read number. Finally we checked whether this effect appears in photometry. We performed a similar read-chopping test using SPARS10, 13-read ramps of the standard star GD-153, in which we took photometry of the star in each FLT composed of the new number of reads. We found that the photometry is indeed stable (within 1% of the value found in the 13th read) once the number of reads hits four to six (see Figure A4).

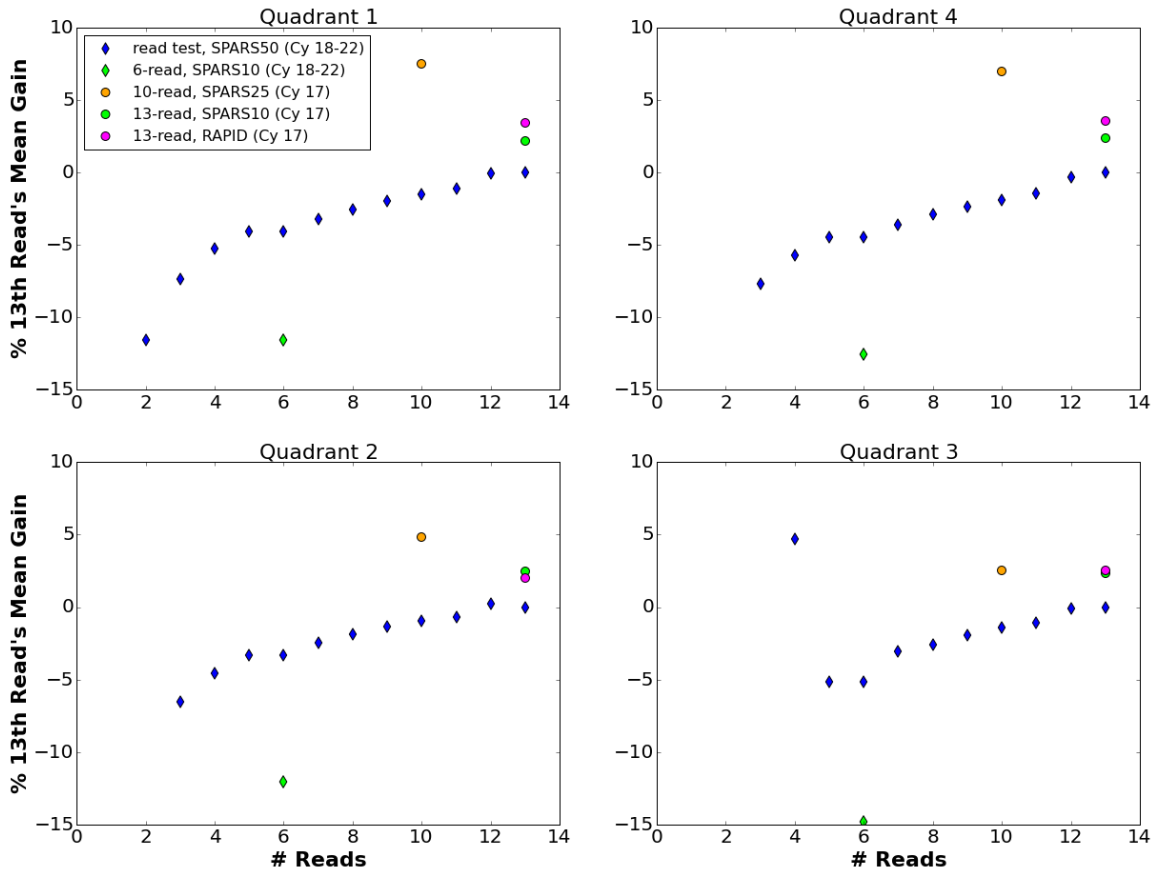

Figure 8. Percent change from the 13th read's average gain for the SPARS50 data. The blue diamond points are means of all the SPARS50 ramps, recalibrated with successively decreasing numbers of reads; thus the marker at read 13 delineates the "original" mean. Cycle 17 (circles) were observed with different filters and sampling sequences from the observing cadence used from Cycle 18 onward, and are plotted for completeness. Because of these fundamental distinctions, it is not surprising that their gain measurements do not line up with those for the SPARS50 reads.

3.4 Applying the 2014 Non-Linearity Correction

We re-calibrated all the data, both short and long flats, with an updated (generated in 2014) non-linearity correction, which is not yet in the CALWF3 pipeline (Hilbert 2014). Running the scripts on these data with identical settings used on the present CALWF3-corrected data (which uses a correction generated in 2008), we find the gain values from the 2014-corrected data are lower by ~1%. We would expect lower values because the 2014 non-linearity correction should allow a better linear fit. A poorer correction results in a fit that is too low, and because gain is the reciprocal of the slope, a lower slope yields a higher gain. Therefore, a better fit will push up the slope to the "ideal" value and yield a lower gain, just as we see. For further discussion of the pipeline non-linearity correction see the Analysis section of WFC3 ISR 2008-50 by B. Hilbert. For graphical comparisons of the effect of the different non-linearity correction solutions on the IR gain measurements, see Figures 9, 10, and 11.

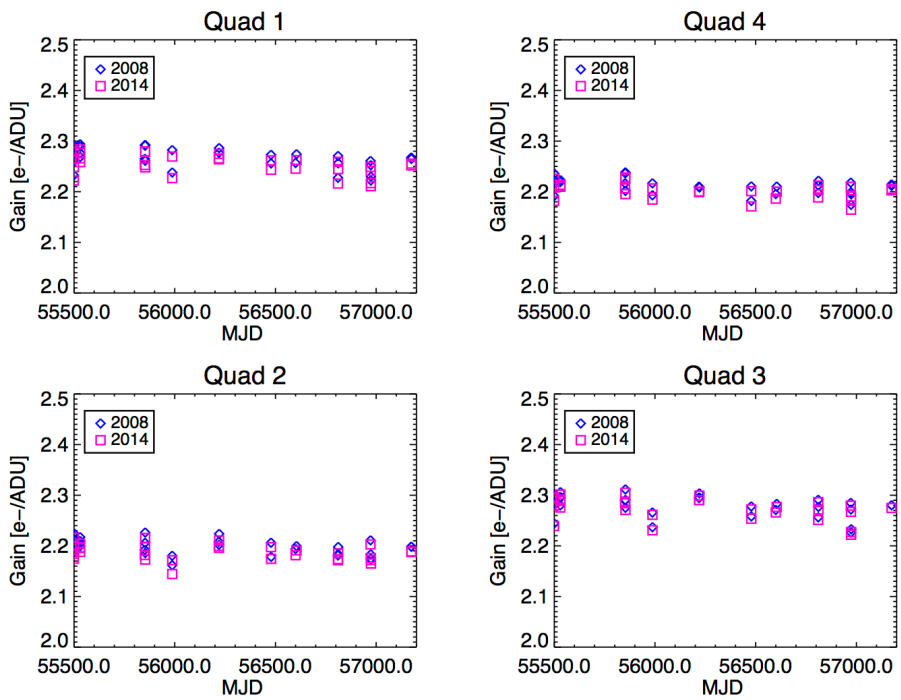

Figure 9. Comparison of the 13-read, SPARS50 gain values with the current (2008) and the 2014 non-linearity correction applied. As expected, the 2014 gain values are slightly lower. Standard deviations for each quadrant's gain are about 0.02 e-/ADU.

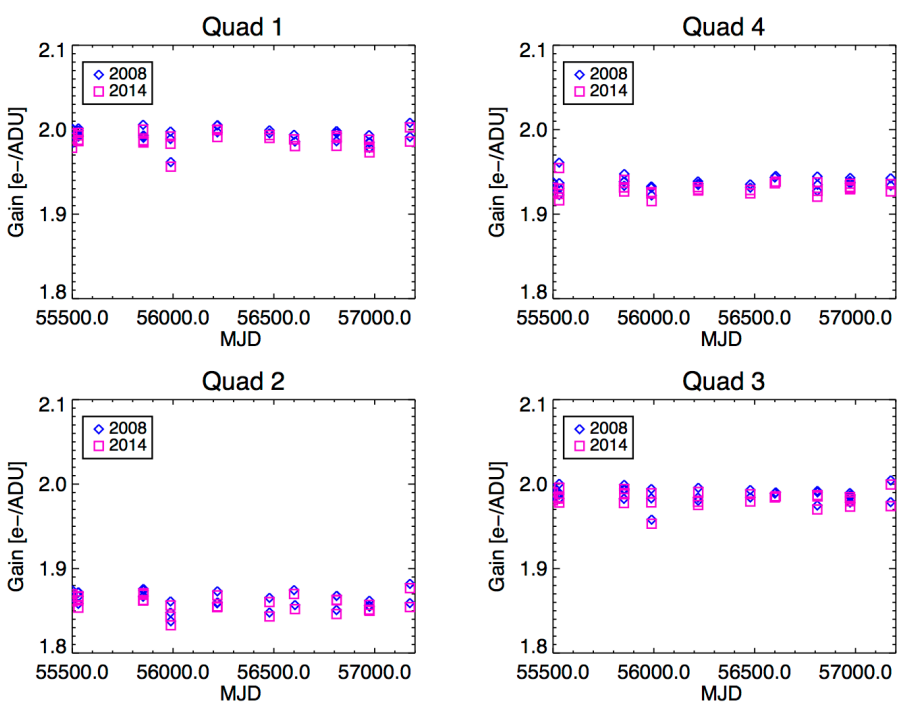

Figure 10. Comparison of the 6-read, SPARS10 gain values with the current (2008) and the 2014 non-linearity correction applied. As with the 13-read ramps, the gain values calculated with the 2014 correction are slightly lower. As of fall 2015, the 2014 correction is not yet in the pipeline.

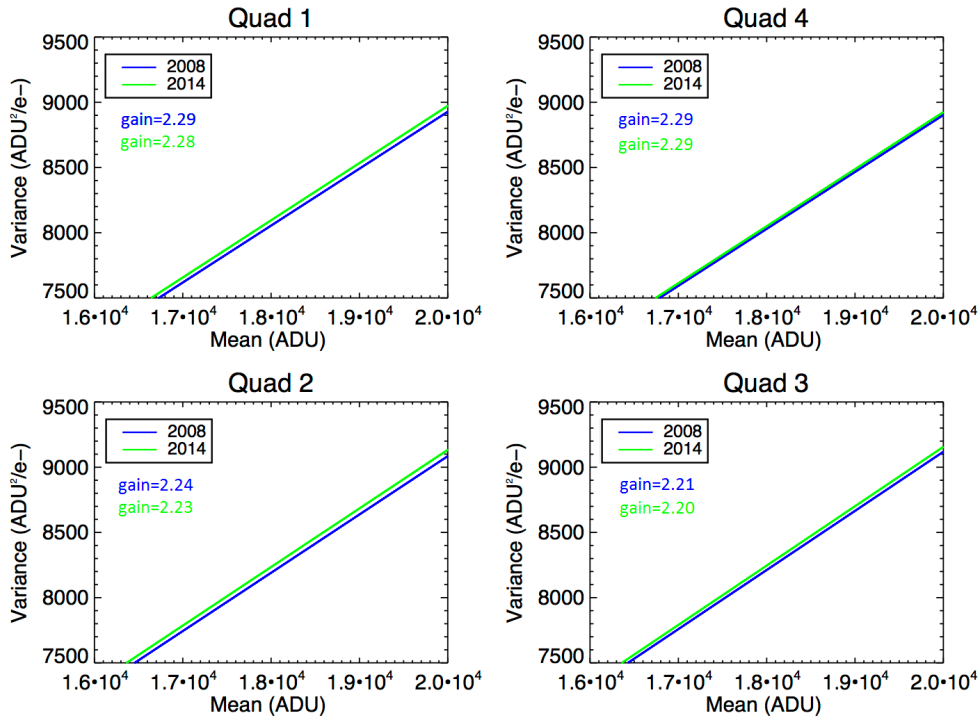

Figure 11. The two lines, zoomed in, compare the least-squares linear fits to the mean-variance plots with the current (2008) and the 2014 non-linearity corrections applied. This 13-read, SPARS50 ramp pair is *ibve03lnq_ima.fits* and *ibve04mpq_ima.fits*.

3.5 The Final Gain

The last published gain values were 2.31-2.41 e-/ADU (Hilbert 2008). But we cannot directly compare our results to Hilbert's values – obtained prior to launch – because our visit structure, observing cadence, our methods of measurement, our calibration files, and so on, are different. Instead, we here establish a new baseline, using observations from 2010 onward processed with our own method so that the analysis technique is standardized and the resultant gain values can be inter-compared.

To obtain our baseline values, we take the average of each half-year group (which can consist of at most eight visits). We discard the outlier from the pair *ibve15kjq_ima.fits* and *ibve16o1q_ima.fits* (image with extreme persistence). We take an average over the entire dataset to achieve a final gain measurement for each quadrant, listed in the final row of Table 3. The gain for each quadrant appears stable, with each individual measurement within 1-2% of the overall average.

Following the convention established in the previous IR gain ISRs (Hilbert 2007 and Hilbert 2008) we also report the overall average for the gain calculated without the inter-pixel capacitance (IPC) correction: 2.50, 2.45, 2.43, 2.51 ± 0.02 e-/ADU for quadrants 1, 2, 3, 4, respectively. We discuss the IPC correction in Section 3.2.

Table 3. Average gain values and their standard deviations (italics) for the 2008 and 2014 non-linearity corrections. Gain values are measured from 13-read (~600 sec), SPARS50 exposures with the F126N filter. To the significant digits displayed, the standard deviation for the 2014 correction is the same as for 2008, and not repeated in the 2014 columns to reduce clutter. We take the average of all the data (*not* the average of the averages) in the final row – these are our final values for the gain.

Cycle	**Gain Quad 1 (e-/ADU)**		**Gain Quad 2 (e-/ADU)**		**Gain Quad 3 (e-/ADU)**		**Gain Quad 4 (e-/ADU)**	
	2008	**2014**	**2008**	**2014**	**2008**	**2014**	**2008**	**2014**
18, Oct 2010	2.26 *0.03*	2.25	2.22 *0.02*	2.21	2.21 *0.02*	2.20	2.28 *0.03*	2.28
18, Nov 2010	2.28 *0.01*	2.27	2.22 *0.00*	2.21	2.21 *0.01*	2.20	2.29 *0.01*	2.29
19, Oct 2011	2.28 *0.02*	2.26	2.22 *0.02*	2.21	2.21 *0.02*	2.19	2.29 *0.01*	2.29
19, Mar 2012	2.26 *0.03*	2.25	2.21 *0.02*	2.20	2.17 *0.01*	2.16	2.25 *0.02*	2.25
20, Oct 2012	2.28 *0.01*	2.27	2.21 *0.00*	2.20	2.21 *0.01*	2.20	2.30 *0.01*	2.30
20, Jul 2013	2.26 *0.01*	2.25	2.20 *0.02*	2.19	2.20 *0.02*	2.19	2.27 *0.01*	2.26
21, Nov 2013	2.27 *0.01*	2.25	2.20 *0.01*	2.19	2.20 *0.00*	2.19	2.28 *0.01*	2.27
21, Jun 2014	2.25 *0.02*	2.24	2.21 *0.01*	2.20	2.19 *0.01*	2.18	2.28 *0.02*	2.27
22, Nov 2014	2.24 *0.02*	2.23	2.20 *0.02*	2.19	2.19 *0.02*	2.18	2.25 *0.03*	2.25
22, Jun 2015	2.27 *0.01*	2.25	2.21 *0.00*	2.20	2.20 *0.01*	2.19	2.27 *0.02*	2.27
Overall Average	**2.27** ***0.02***	**2.25**	**2.21** ***0.01***	**2.20**	**2.20** ***0.02***	**2.19**	**2.28** ***0.02***	**2.27**

4.0 Conclusions

We have described the IR gain's observation program, data reduction, and analysis methods. We made a case for setting more restrictions on our observations in future calibration proposals, such that one ramp in a pair is always observed within 24 hours of the other.

We report gain measurements of 2.27, 2.21, 2.20, 2.28 e-/ADU, with ~0.02 e-/ADU uncertainty, for quadrants 1, 2, 3, 4, respectively. The 2014 non-linearity correction (not yet implemented in the pipeline) alters these values by a negligible <1%. Because any changes to the gain will have implications to the overall health of the WFC3/IR detector, it will continue to be sampled twice each observing cycle as part of the standard calibration plan.

We also identified two phenomena that require further analysis outside the scope of this report. First, we were surprised to find persistence in 1/3 of our 13-read flats that did not appear in the preceding darks or six-read flats, despite that the 13-read flats do not go over 14,000 DN/pix, which had been thought to be a safe level to avoid such "burped" persistence affects. Further investigation is underway. We note that the persisting objects were so small that, save in one exceptional case, our gain measurements did not seem to be offset. Second, we found that the measured gain value drifted by ~5% depending on how many reads were used for the assessment. We've traced the behavior to a drift in the variance of the differenced ramps (i.e., a ~30% increase from six reads to 13), while the means (measured in countrates) of the summed ramps drifted by <<1% across the reads. It is not an issue for our gain calculation as long as we consistently use the 13-read flats, and we will attempt to understand why this trend in variance occurs.

Acknowledgements

We thank Knox Long for his many helpful suggestions in his review of this report. We also thank Russell Ryan for his help with the 'read-chopping' script.

References

Baggett, S. 2009, WFC3 SMOV Proposals 11423/ 11543: IR FSM and Lamp Checks, WFC3 ISR 2009-28

Bourque, M. and Baggett, S. 2013, WFC3/UVIS Bowtie Monitor, WFC3 ISR 2013-09

Dressel, L. 2015, Wide Field Camera 3 Instrument Handbook, Version 7.0, (Baltimore: STScI)

Hilbert, B. 2014, Updated non-linearity calibration method for WFC3/IR, WFC3 ISR 2014-17

Hilbert, B. 2008, WFC3 TV3 Testing: IR Gain Results, WFC3 ISR 2008-50

Hilbert, B. 2007, WFC3 TV2 Testing: IR Gain Results, WFC3 ISR 2007-28

Hilbert, B. 2005, Results of the WFC3 Thermal Vacuum Testing: IR Channel Gain, WFC3 ISR 2005-14

Hilbert, B. and McCullough, P. 2011, Interpixel Capacitance in the IR Channel: Measurements Made on Orbit, WFC3 ISR 2011-10

Long, K., Baggett, S., Deustua, S., and Riess, A. 2010, WFC3/IR Persistence as Measured in Cycle 17 using Tungsten Lamp Exposures, WFC3 ISR 2010-17

McCullough, P. 2008, Inter-pixel capacitance: prospects for deconvolution, WFC3 ISR 2008-26

Rajan, A. et al. 2010, WFC3 Data Handbook, Version 2.1, (Baltimore: STScI)

Ryan, R.E., Jr. and Baggett, S.M. 2015, The Internal Flat Fields for WFC3/IR, WFC3 ISR 2015-11

Appendix

Table A1. All ramp pairs with six reads taken at the SPARS10 sample sequence (the short, warm-up flats). Gain values are listed for both the 2008 (currently in CALWF3) and the 2014 non-linearity corrections. Uncertainties are <0 .01 e-/ADU.

				Gain 1		Gain 2		Gain 3		Gain 4	
Image a	**Image b**	**MJD a**	**MJD b**	**2008**	**2014**	**2008**	**2014**	**2008**	**2014**	**2008**	**2014**
ibm801goq_ima.fits	ibm802h9q_ima.fits	55499.20	55499.27	1.98	1.98	1.94	1.93	1.87	1.87	2.00	1.99
ibm803hrq_ima.fits	ibm804icq_ima.fits	55499.34	55499.40	2.00	2.00	1.94	1.93	1.87	1.87	1.99	1.98
ibm805k6q_ima.fits	ibm806ldq_ima.fits	55499.68	55499.90	2.00	1.99	1.93	1.93	1.87	1.87	1.99	1.98
ibm807p8q_ima.fits	ibm808peq_ima.fits	55500.32	55500.39	2.00	2.00	1.93	1.92	1.87	1.86	1.99	1.98
ibm809jyq_ima.fits	ibm810ldq_ima.fits	55530.15	55530.22	1.99	1.99	1.96	1.95	1.86	1.85	1.99	1.98
ibm811mkq_ima.fits	ibm812ncq_ima.fits	55530.29	55530.35	2.00	1.99	1.93	1.92	1.87	1.87	1.99	1.98
ibm813osq_ima.fits	ibm814p8q_ima.fits	55530.67	55530.74	2.00	2.00	1.92	1.92	1.87	1.86	2.00	2.00
ibm815plq_ima.fits	ibm816pwq_ima.fits	55530.81	55530.87	1.99	1.99	1.94	1.93	1.87	1.87	1.98	1.98
ibve01e5s_ima.fits	ibve02jbq_ima.fits	55851.51	55852.25	2.01	2.00	1.94	1.93	1.87	1.86	1.98	1.98
ibve03lmq_ima.fits	ibve04moq_ima.fits	55852.77	55852.93	1.99	1.99	1.93	1.93	1.88	1.87	2.00	1.99
ibve05ohq_ima.fits	ibve06q0q_ima.fits	55853.10	55853.25	1.99	1.98	1.94	1.93	1.87	1.86	1.99	1.99
ibve07qqq_ima.fits	ibve08rmq_ima.fits	55853.40	55853.68	1.99	1.99	1.95	1.94	1.87	1.87	1.99	1.99
ibve11vzq_ima.fits	ibve12xlq_ima.fits	55987.26	55987.39	1.99	1.98	1.93	1.92	1.84	1.84	1.98	1.98
ibve13yqq_ima.fits	ibve14gqq_ima.fits	55987.52	55988.20	2.00	1.99	1.93	1.93	1.86	1.86	1.99	1.99
ibve15kiq_ima.fits	ibve16o0q_ima.fits	55988.94	55989.40	1.96	1.96	1.92	1.92	1.84	1.83	1.96	1.95
ic5601aeq_ima.fits	ic5602aqq_ima.fits	56220.27	56220.34	2.01	2.00	1.94	1.93	1.86	1.86	2.00	1.99
ic5605pvq_ima.fits	ic5606wpq_ima.fits	56218.73	56219.47	2.01	2.00	1.94	1.93	1.86	1.85	1.98	1.98
ic5607xlq_ima.fits	ic5608xpq_ima.fits	56219.74	56219.77	2.00	1.99	1.93	1.93	1.87	1.87	1.98	1.98
ic5613y8q_ima.fits	ic5614yeq_ima.fits	56478.15	56478.17	2.00	1.99	1.94	1.93	1.87	1.86	1.99	1.99
ic5615yvq_ima.fits	ic5616ecq_ima.fits	56478.28	56479.21	2.00	1.99	1.93	1.92	1.85	1.84	1.98	1.98
icfi01b2q_ima.fits	icfi02boq_ima.fits	56600.10	56600.23	1.99	1.99	1.94	1.94	1.87	1.87	1.99	1.98
icfi07dtq_ima.fits	icfi08egq_ima.fits	56604.55	56604.68	1.99	1.98	1.95	1.94	1.86	1.85	1.99	1.99
icfi09eeq_ima.fits	icfi10fgq_ima.fits	56810.55	56810.76	1.99	1.98	1.93	1.92	1.85	1.85	1.97	1.97
icfi11fnq_ima.fits	icfi12ieq_ima.fits	56810.82	56811.16	2.00	1.99	1.94	1.94	1.87	1.86	1.99	1.99
icfi15krq_ima.fits	icfi16laq_ima.fits	56811.62	56811.70	2.00	1.99	1.93	1.93	1.87	1.86	1.99	1.99
icpq01h5q_ima.fits	icpq02hdq_ima.fits	56972.22	56972.37	1.99	1.99	1.94	1.93	1.86	1.85	1.99	1.98
icpq03mfq_ima.fits	icpq04n8q_ima.fits	56973.18	56973.37	1.99	1.98	1.94	1.93	1.86	1.85	1.98	1.97
icpq05oqq_ima.fits	icpq06spq_ima.fits	56973.53	56974.18	1.98	1.98	1.94	1.94	1.86	1.86	1.98	1.98
icpq07tgq_ima.fits	icpq08xqq_ima.fits	56974.39	56975.31	1.98	1.97	1.94	1.93	1.86	1.85	1.99	1.98
icpq09fpq_ima.fits	icpq10haq_ima.fits	57174.62	57174.79	2.01	2.00	1.94	1.94	1.86	1.85	1.98	1.97
icpq11ihq_ima.fits	icpq12laq_ima.fits	57174.96	57175.53	1.99	1.99	1.93	1.93	1.88	1.88	2.00	2.00
icpq17cyq_ima.fits	icpq18i2q_ima.fits	57201.15	57202.66	1.99	1.98	1.92	1.92	1.85	1.85	1.99	1.98
icpq19boq_ima.fits	icpq20cjq_ima.fits	57202.09	57202.13	1.99	1.98	1.93	1.93	1.86	1.86	1.98	1.98

Table A2. Same as Table A1, except these ramp pairs have 13 reads taken at the SPARS50 sample sequence (the long flats). Uncertainties are <0 .01 e-/ADU.

				Gain 1		Gain 2		Gain 3		Gain 4	
Image a	**Image b**	**MJD a**	**MJD b**	**2008**	**2014**	**2008**	**2014**	**2008**	**2014**	**2008**	**2014**
ibm801gpq_ima.fits	ibm802haq_ima.fits	55499.20	55499.27	2.23	2.22	2.19	2.18	2.19	2.17	2.24	2.24
ibm803hsq_ima.fits	ibm804idq_ima.fits	55499.34	55499.40	2.28	2.27	2.22	2.21	2.23	2.21	2.30	2.30
ibm805k7q_ima.fits	ibm806leq_ima.fits	55499.68	55499.90	2.26	2.25	2.22	2.21	2.20	2.18	2.28	2.28
ibm807p9q_ima.fits	ibm808pfq_ima.fits	55500.32	55500.39	2.29	2.28	2.24	2.23	2.22	2.20	2.30	2.29
ibm809jzq_ima.fits	ibm810leq_ima.fits	55530.16	55530.22	2.28	2.27	2.22	2.21	2.21	2.20	2.28	2.28
ibm811mlq_ima.fits	ibm812ndq_ima.fits	55530.29	55530.36	2.29	2.28	2.22	2.21	2.22	2.20	2.29	2.29
ibm813otq_ima.fits	ibm814p9q_ima.fits	55530.67	55530.74	2.29	2.28	2.22	2.21	2.21	2.20	2.31	2.30
ibm815pmq_ima.fits	ibm816pxq_ima.fits	55530.82	55530.87	2.27	2.26	2.22	2.21	2.20	2.19	2.30	2.29
ibve01e6s_ima.fits	ibve02jcq_ima.fits	55851.51	55852.25	2.27	2.25	2.22	2.21	2.19	2.18	2.29	2.28
ibve03lnq_ima.fits	ibve04mpq_ima.fits	55852.77	55852.93	2.29	2.28	2.24	2.23	2.21	2.20	2.29	2.29
ibve05oiq_ima.fits	ibve06q1q_ima.fits	55853.10	55853.25	2.29	2.28	2.24	2.23	2.23	2.22	2.31	2.30
ibve07qrq_ima.fits	ibve08rnq_ima.fits	55853.40	55853.68	2.26	2.25	2.20	2.20	2.19	2.17	2.28	2.27
ibve11w0q_ima.fits	ibve12xmq_ima.fits	55987.26	55987.39	2.28	2.27	2.22	2.21	2.18	2.17	2.27	2.26
ibve13yrq_ima.fits	ibve14grq_ima.fits	55987.52	55988.21	2.24	2.23	2.19	2.18	2.16	2.14	2.24	2.23
ibve15kjq_ima.fits	ibve16o1q_ima.fits*	55988.94	55989.40	1.91	1.90	1.94	1.93	1.95	1.94	1.93	1.93
ic5601afq_ima.fits	ic5602arq_ima.fits	56220.27	56220.34	2.29	2.27	2.21	2.20	2.22	2.21	2.30	2.29
ic5605pwq_ima.fits	ic5606wqq_ima.fits	56218.73	56219.47	2.28	2.27	2.21	2.20	2.21	2.20	2.29	2.29
ic5607xmq_ima.fits	ic5608xqq_ima.fits	56219.74	56219.77	2.28	2.26	2.21	2.20	2.20	2.20	2.30	2.29
ic5613y9q_ima.fits	ic5614yfq_ima.fits	56478.15	56478.17	2.27	2.26	2.21	2.20	2.21	2.20	2.28	2.27
ic5615ywq_ima.fits	ic5616edq_ima.fits	56478.28	56479.21	2.26	2.24	2.18	2.17	2.18	2.17	2.26	2.25
icfi01b3q_ima.fits	icfi02bpq_ima.fits	56600.10	56600.23	2.26	2.25	2.20	2.19	2.19	2.18	2.27	2.27
icfi07duq_ima.fits	icfi08ehq_ima.fits	56604.56	56604.68	2.27	2.26	2.21	2.20	2.20	2.19	2.28	2.28
icfi09efq_ima.fits	icfi10fhq_ima.fits	56810.55	56810.77	2.23	2.22	2.20	2.19	2.18	2.17	2.26	2.25
icfi11foq_ima.fits	icfi12ifq_ima.fits	56810.82	56811.16	2.27	2.26	2.21	2.20	2.18	2.17	2.29	2.29
icfi15ksq_ima.fits	icfi16lbq_ima.fits	56811.62	56811.70	2.26	2.24	2.22	2.19	2.20	2.19	2.28	2.27
icpq01h6q_ima.fits	icpq02heq_ima.fits	56972.22	56972.37	2.26	2.25	2.22	2.21	2.21	2.20	2.29	2.28
icpq03mgq_ima.fits	icpq04n9q_ima.fits	56973.18	56973.37	2.25	2.24	2.20	2.19	2.18	2.18	2.27	2.27
icpq05orq_ima.fits	icpq06sqq_ima.fits	56973.53	56974.18	2.22	2.21	2.17	2.16	2.17	2.17	2.23	2.22
icpq07thq_ima.fits	icpq08xrq_ima.fits	56974.39	56975.31	2.23	2.22	2.19	2.19	2.17	2.17	2.23	2.23
icpq09fqq_ima.fits	icpq10hbq_ima.fits	57174.62	57174.80	2.27	2.26	2.21	2.21	2.20	2.19	2.28	2.27
icpq11iiq_ima.fits	icpq12lbq_ima.fits	57174.96	57175.53	2.26	2.25	2.21	2.20	2.20	2.19	2.28	2.27
icpq17czq_ima.fits	icpq18i3q_ima.fits	57202.16	57202.66	2.28	2.26	2.21	2.20	2.19	2.18	2.28	2.28
icpq19bpq_ima.fits	icpq20ckq_ima.fits	57202.09	57202.13	2.26	2.25	2.21	2.20	2.20	2.19	2.25	2.24

* This image showed full-frame persistence from a star field (adding between a few 10s to a few 100s DN per affected pixel), and is likely the cause of its low gain measurements. We therefore throw out these measurements from our final calculation.

Table A3. Persistence flags for each quadrant of each ramp used in the gain measurements. Most persistence events were small and faint ("flag=1"), and only became obvious in the ramps after they had been ratio'd. As discussed in Section 3.3, persistence has no obvious effect on the gain measurement, except in the abnormally bad case of *ibve16o1q_ima.fits.*

Image	MJD	Flag 1	Flag 2	Flag 3	Flag 4	Comments
ibm801gpq_ima.fits	55499.2	0	0	0	0	
ibm802haq_ima.fits	55499.27	0	0	0	0	Ratio ramp
ibm803hsq_ima.fits	55499.34	0	0	0	0	
ibm804idq_ima.fits	55499.4	0	0	0	0	
ibm805k7q_ima.fits	55499.68	0	0	0	0	
ibm806leq_ima.fits	55499.9	1	0	0	1	Two grism streaks
ibm807p9q_ima.fits	55500.32	1	0	0	1	Two grism streaks, fainter
ibm808pfq_ima.fits	55500.39	1	0	0	1	Two grism streaks, even fainter
ibm809jzq_ima.fits	55530.16	0	0	0	0	Flat field features pop out
ibm810leq_ima.fits	55530.22	0	0	0	0	
ibm811mlq_ima.fits	55530.29	0	0	0	0	
ibm812ndq_ima.fits	55530.36	0	0	0	0	
ibm813otq_ima.fits	55530.67	0	0	0	1	Glinting in corner
ibm814p9q_ima.fits	55530.74	0	0	0	0	
ibm815pmq_ima.fits	55530.82	0	0	0	0	
ibm816pxq_ima.fits	55530.87	0	0	0	0	
ibve01e6s_ima.fits	55851.51	1	1	1	0	Three grism streaks
ibve02jcq_ima.fits	55852.25	1	1	1	0	Three grism streaks, fainter
ibve03lnq_ima.fits	55852.77	1	1	1	0	Three grism streaks, fainter
ibve04mpq_ima.fits	55852.93	1	1	1	0	Three grism streaks, fainter
ibve05oiq_ima.fits	55853.1	1	1	1	0	Three grism streaks, even fainter
ibve06q1q_ima.fits	55853.25	1	1	0	0	Three grism streaks, even fainter
ibve07qrq_ima.fits	55853.4	1	2	0	0	Five grism streaks, two from previous
ibve11w0q_ima.fits	55987.26	0	0	0	0	Flat field features pop out
ibve12xmq_ima.fits	55987.39	0	0	0	0	Flat field features pop out
ibve13yrq_ima.fits	55987.52	0	0	0	0	
ibve14grq_ima.fits	55988.21	0	0	0	1	Glinting in corner
ibve15kjq_ima.fits	55988.94	2	2	0	2	Glinting; four grism streaks
ibve16o1q_ima.fits	55989.4	3	3	3	3	Persisting star field all across detector, grism streaks fainter
ic5601afq_ima.fits	56220.27	1	0	1	1	Glinting in corner. four persisting stars
ic5602arq_ima.fits	56220.34	2	2	0	1	Glinting
ic5605pwq_ima.fits	56218.73	1	1	0	0	Two grism streaks
ic5606wqq_ima.fits	56219.47	1	1	0	0	Three grism streaks, fainter
ic5607xmq_ima.fits	56219.74	0	0	0	0	
ic5608xqq_ima.fits	56219.77	0	0	0	0	
ic5613y9q_ima.fits	56478.15	0	0	0	0	Flat field features pop out

ic5614yfq_ima.fits	56478.17	0	0	0	0	
ic5615ywq_ima.fits	56478.28	2	2	0	1	Glinting
ic5616edq_ima.fits	56479.21	0	0	0	0	Flat field features pop out
icfi01b3q_ima.fits	56600.1	2	2	0	0	Glinting
icfi02bpq_ima.fits	56600.23	0	0	0	0	
icfi07duq_ima.fits	56604.56	1	1	1	1	Many faint grism streaks, two very bright at center
icfi08ehq_ima.fits	56604.68	2	1	0	1	Glinting; grism streaks fainter
icfi09efq_ima.fits	56810.55	1	0	0	0	Two grism streaks
icfi10fhq_ima.fits	56810.77	1	0	0	0	Two grism streaks
icfi11foq_ima.fits	56810.82	1	0	0	0	Two grism streaks
icfi12ifq_ima.fits	56811.16	2	2	2	2	Two diagonal earth flat streaks, two grism streaks fainter
icfi15ksq_ima.fits	56811.62	2	2	2	2	Two diagonal earth flat streaks fainter, faint star field
icfi16lbq_ima.fits	56811.7	2	2	2	2	Two diagonal earth flat streaks fainter, faint star field
icpq01h6q_ima.fits	56972.22	1	0	0	0	Two grism streaks
icpq02heq_ima.fits	56972.37	1	0	0	0	Two grism streaks
icpq03mgq_ima.fits	56973.18	1	1	0	0	Galaxies? Two grism streaks fainter
icpq04n9q_ima.fits	56973.37	0	1	0	0	Galaxies fainter
icpq05orq_ima.fits	56973.53	0	1	0	0	Galaxies
icpq06sqq_ima.fits	56974.18	0	1	0	0	Galaxies fainter
icpq07thq_ima.fits	56974.39	2	2	0	0	Glinting
icpq08xrq_ima.fits	56975.31	2	2	0	0	Glinting
icpq09fqq_ima.fits	57174.62	0	0	0	0	
icpq10hbq_ima.fits	57174.8	0	0	0	0	
icpq11iiq_ima.fits	57174.96	0	0	0	0	
icpq12lbq_ima.fits	57175.53	0	0	0	0	
icpq17czq_ima.fits	57202.16	0	0	0	0	
icpq18i3q_ima.fits	57202.66	0	1	0	0	Two persisting stars
icpq19bpq_ima.fits	57202.09	0	0	0	0	

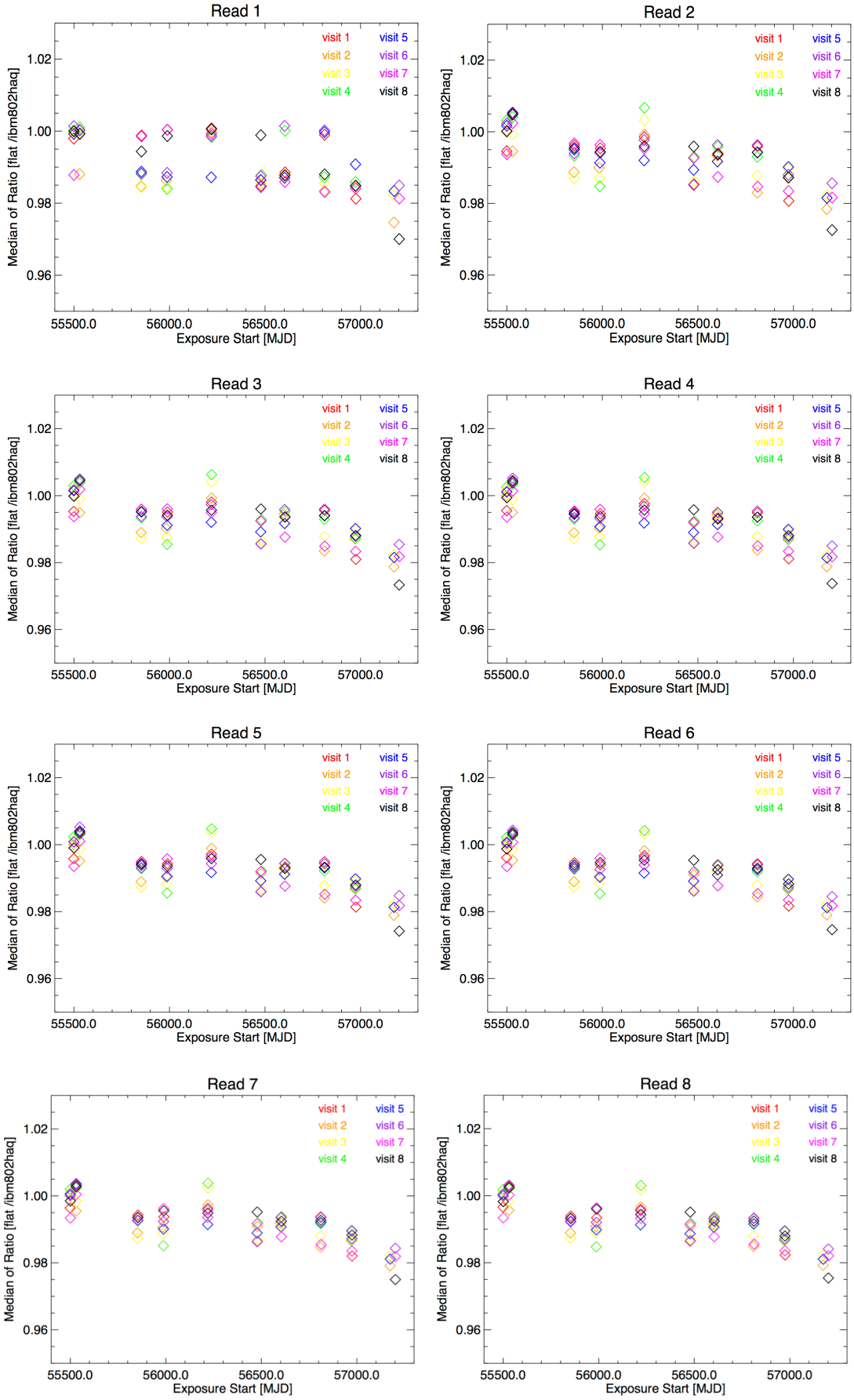
Read 1
Read 2
Read 3
Read 4
Read 5
Read 6
Read 7
Read 8
visit 1
visit 2
visit 3
visit 4
visit 5
visit 6
visit 7
visit 8
Median of Ratio [flat /ibm802haq]
1.02
1.00
0.98
0.96
55500.0
56000.0
56500.0
57000.0
Exposure Start [MJD]

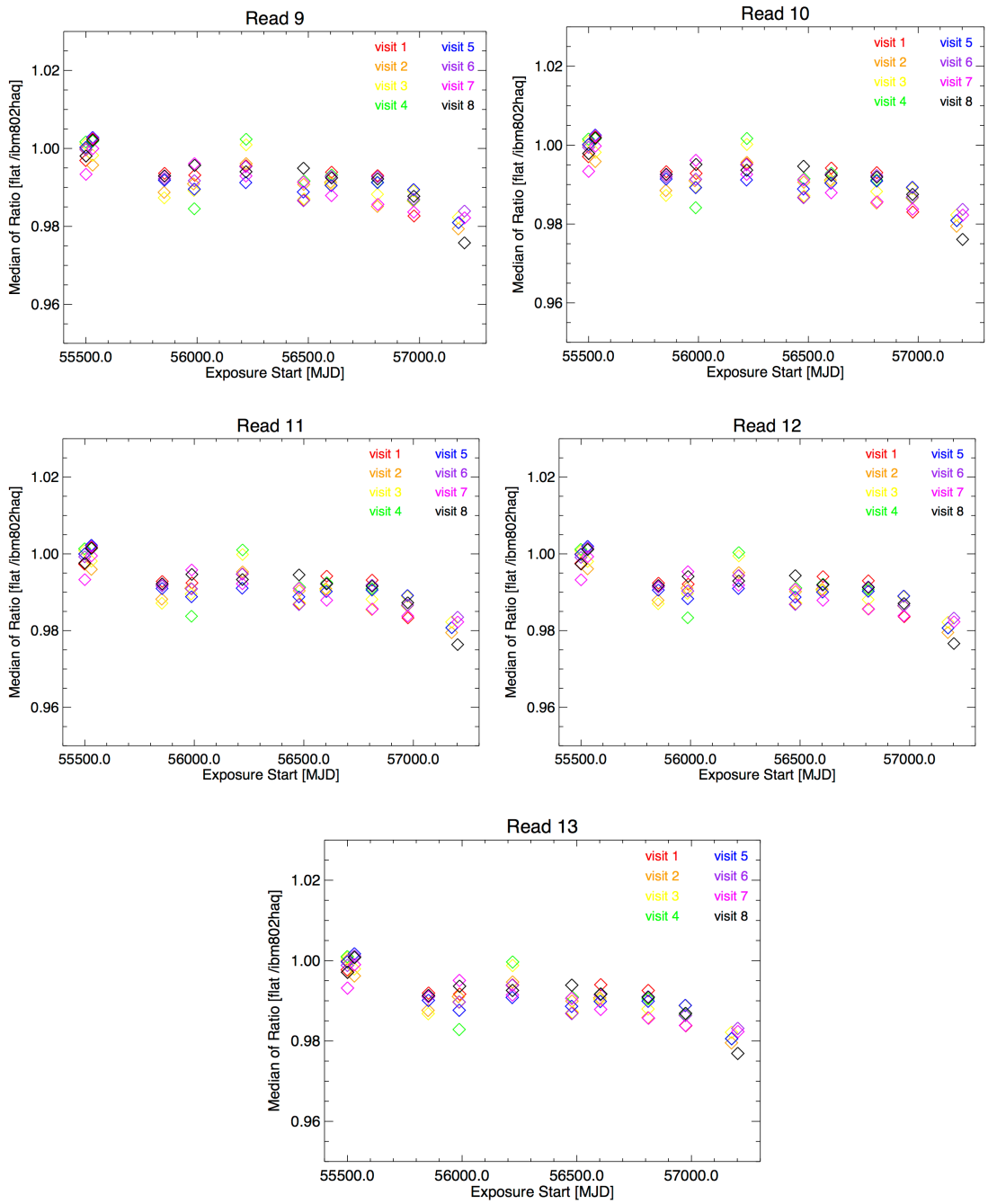

Figure A1. Medians of the long (13-read) flats' ratio to the Cycle 18, Program 12350 flat *ibm801goq_ima.fits*. Same as Figure 3, each panel shows a different read, and each color shows a different visit in the eight-visit per six-month observation cadence. And just as in Figure 3, we see a decrease in the lamp's flux output. But more noticeable here than in Figure 3, we see that the plot points' scatter tightens as the reads increase. This is likely because of the increase in S/N. The data taken around 56000 MJD show the greatest scatter even in the 13th read; this date correlates well with the worst persistence events found in the dataset (see Table A3). Note that we do not have gain measurements for every point displayed, since some of them were unpairable under the 24-hour limit.

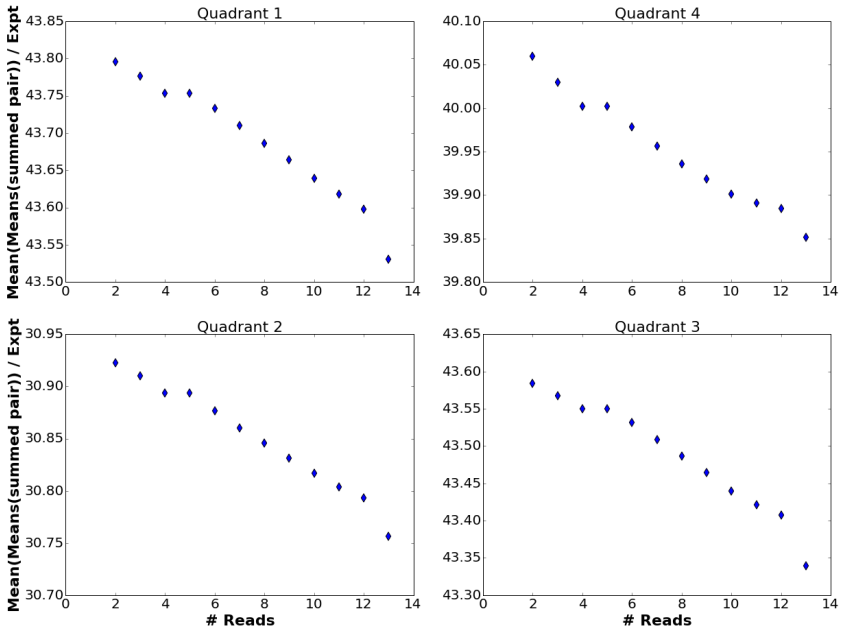

Figure A2. Mean of the means (of the summed ramp pair) plotted against number of reads used in the final IMA for the ramp pair *icfi15ksq_ima.fits* and *icfi16lbq_ima.fits*. The means decrease by ~0.5% with number of ramps used. This may because of the imperfection of the non-linearity correction. The decline, however, is too small to account for the upward trend in gain versus number of used reads shown in Figure 8. See Figure A3 for discussion on the variance.

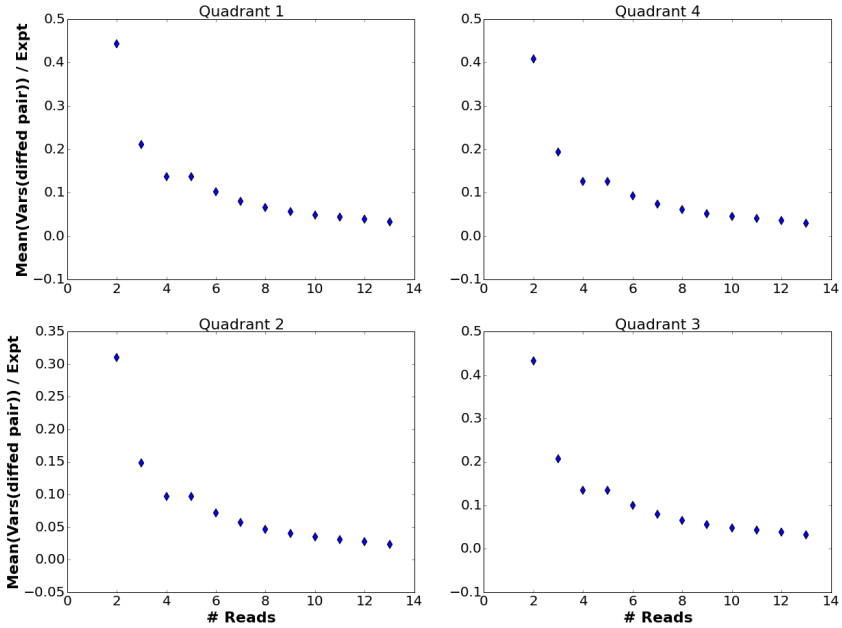

Figure A3. Mean of the variances (of the differenced ramp pair) plotted against number of reads used in the final IMA for the ramp pair *icfi15ksq_ima.fits* and *icfi16lbq_ima.fits*. It is curious that the variance shows such a dramatic decline, by as much as ~90% from the two-read IMA pair to the 13-read IMA pair. Some of the initial decline may be due to reset effects in the first read or two. Whatever its cause, this decline in variance does explain the increase in Figure 8's plot of gain versus number of used reads. We are investigating this further.

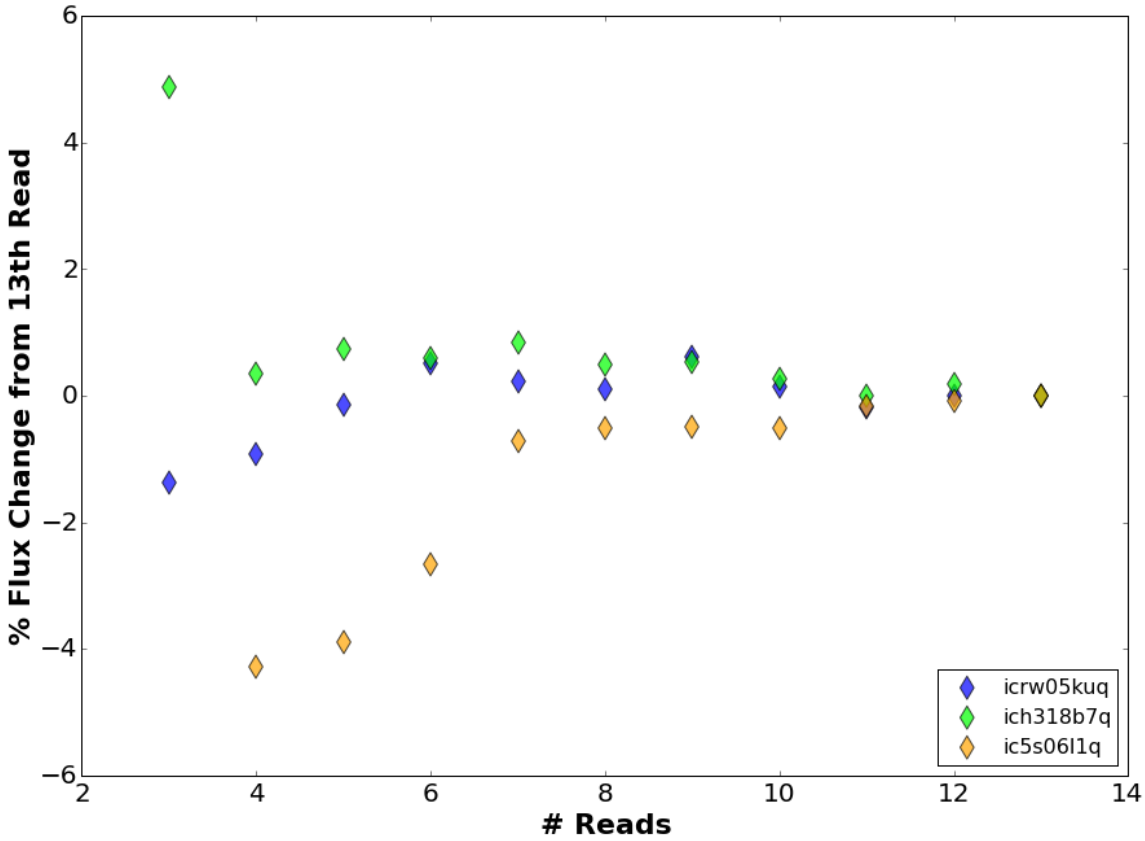

Figure A4. Photometry for three observations of white dwarf GD-153 (all F167N, SPARS10, 13-read subarrays) from WFC3/IR photometric calibration programs. Percent difference from the 13th read of each individual star is plotted against number of reads used in the recalibrated IMA. Although the photometry for one target stabilized to 1% after 6 reads (longer than might be expected if reset effects are driving the flux changes in early reads) the other two sources show photometry stable to better than 1% after the first one to two reads. Based on this and the results shown in Figures A1 and A2, we therefore conclude that the decline in the plot of gain versus number of used reads (Figure 8) is unique to the flat fields and the gain calculation itself (the variance of the differenced ramps in particular), and is not impacting photometry.